

1 Organic geochemistry evidence for wildfire and elevated
2 pO_2 at the Frasnian–Famennian boundary

3 **Zeyang Liu¹, Hui Tian^{1*}, David Selby², Jianfang Hu¹, and D. Jeffrey Over³**

4 ¹ State Key Laboratory of Organic Geochemistry, CAS Center for Excellence in Deep Earth
5 Science, Guangzhou Institute of Geochemistry, Chinese Academy of Sciences, Guangzhou 510640,
6 China

7 ²Department of Earth Sciences, University of Durham, Durham DH1 3LE, UK

8 ³Department of Geological Sciences, SUNY College at Geneseo, Geneseo, NY 14454, USA

9 *Corresponding author: Hui Tian (tianhui@gig.ac.cn)

10 **Abstract**

11 The Devonian experienced radiations of plants and animals, as well as a major mass
12 extinction event during the Frasnian–Famennian (F–F) interval. Proposed triggers have
13 been linked to volcanism, extraterrestrial impact, sea-level fluctuations, and climate
14 cooling, etc. However, the nature of the wildfires and its role in the biotic evolution have
15 been rarely investigated for the F–F interval. Here, we report organic geochemistry
16 proxies (*e.g.*, polycyclic aromatic hydrocarbons, PAHs) in three sections from New York
17 (USA) to further investigate the wildfire activity and its potential link with the
18 environmental and biotic perturbations around the F–F interval. The studied intervals are
19 dominated by three-ring PAHs which display an increasing abundance stratigraphically
20 towards the F–F boundary (FFB). An increase of 6-ring over 3-ring PAHs across the FFB
21 is also observed for the studied sections, indicating elevated burning temperature.
22 Additionally, slightly increased plant wax abundance and average chain length values and
23 relatively constant Pr/Ph ratios are observed. Collectively, these results propose an
24 increased burning frequency over the F–F interval caused by elevated pO_2 level, rather
25 than a change in aridity. Terrestrial input only slightly increased across the FFB, and there
26 is limited evidence for ocean anoxia. This correlates with the hypothesis that pCO_2
27 drawdown and climate cooling could have been a driving mechanism of the F–F biocrisis.

28 **Keywords:** atmospheric oxygen level; polycyclic aromatic hydrocarbons; F–F; terrestrial
29 input; pCO_2 drawdown; weathering

30 **1 Introduction**

31 The Earth witnessed dramatic changes during the Devonian. Within these changes,
32 the evolution and widespread rapid terrestrial invasion of plants increased the
33 atmospheric levels of oxygen (pO_2 ; Glasspool and Scott, 2010). The expansion of
34 terrestrial plants provided the habitat and oxygen necessary for the terrestrial evolution
35 of life on land and ultimately led to the appearance of larger body size animals that had a
36 higher oxygen demand (Dahl et al., 2010). In addition to the radiation of life over this
37 period, the Late Devonian also records one of the “big five” mass extinction events – the
38 Frasnian–Famennian (F–F) biocrisis (Stanley, 2016). Possible causes of this catastrophic
39 event have been attributed to, but not limited to, volcanism (Racki et al., 2018),
40 extraterrestrial impact (Claeys et al., 1992, although this has since been refuted by
41 multiple studies, e.g. Percival et al., 2018), ocean anoxia and/or euxinia (e.g., Bond et al.,
42 2004; Bond and Wignall, 2008; Carmichael et al., 2014), sea-level fluctuation (Copper,
43 2002; Johnson et al., 1985), climate cooling (Joachimski et al., 2009; Huang et al., 2018),
44 and orbital forcing (Lu et al., 2021).

45 Wildfires played an important role in regulating the Earth’s environment (Glasspool
46 et al., 2015). In the geological record, fire frequency is closely linked with pO_2 and has
47 been extensively studied for intervals with major climatic and biotic perturbations, such
48 as the Permian–Triassic mass extinction (Shen et al., 2011). In contrast, a wildfire event
49 has been rarely studied for the F–F interval. Previously, the F–F interval has been taken

50 to represent an interval during which wildfire events are sparse (Scott and Glasspool,
51 2006; Rimmer et al., 2015). No fossil charcoal has been found in this interval, despite the
52 availability of terrestrial plants to be burnt (Stein et al., 2012). This leads to the conclusion
53 of a low pO_2 level during the F–F interval such that wildfire activity cannot be sustained
54 (Rimmer et al., 2015). Yet, more recently, fossil charcoal (inertinite) has been reported
55 from five F–F sections in the western New York State (USA), thus providing support for
56 a history of wildfires during the F–F interval (Liu et al., 2020).

57 Despite the observation of inertinite in the New York State F–F sections, the trends
58 in the inertinite abundance profiles are not uniform, which hampered the interpretation of
59 the role of wildfires in the F–F mass extinction, and highlights the need for more
60 comprehensive studies of wildfire events over the F–F interval. Here, we report PAHs
61 data, coupled with Pr/Ph, plant wax abundance and average chain length data from three
62 New York sections to further constrain the timing of wildfire events. The concentrations
63 of PAHs, unlike inertinites, do exhibit trends in changes of fire intensity across the F–F
64 boundary. As such, we discuss the potential link between wildfire events and the biotic
65 and climatic perturbations during the Late Devonian.

66 **2 Samples**

67 In this study, three outcrop sections (Beaver Meadow Creek, BMC; Irish Gulf, IG;
68 Walnut Creek Bank, WCB) from western New York state were investigated (Fig. 1).
69 These records represent slope to basin deposits within the northern Appalachian foreland

70 basin, and are interpreted to be proximal to distal deposits in terms of paleoceanography
71 (see inserted map of Fig. 1) (Sageman et al., 2003). In all three sections, the studied
72 interval is composed of the latest Frasnian–earliest Famennian Hanover Formation and
73 the early Famennian Dunkirk Formation. The Hanover Formation is composed of light
74 gray, silty shales (less than 1 wt. % total organic carbon, TOC) interbedded with black
75 silty shales that are rich in organic matter (~ 1–6 wt. % TOC) and thermally mature (BR_o
76 ~ 0.6 %, solid bitumen reflectance; Liu et al., 2020). Evidence of bioturbation is observed
77 for the grey shale, and hosts poorly preserved brachiopods and bivalves (Over, 1997, 2002;
78 Boyer et al., 2021). The black shales are finely laminated and rich in pyrite, an indication
79 of deposition in an anoxic/dysoxic environment (Boyer et al., 2021; Lash, 2017; Sageman
80 et al., 2003). Overlying the Hanover Formation, the Dunkirk Formation contains thick
81 beds of black shale (Over, et al., 1997). In the stratigraphic records studied here, the F–F
82 boundary is defined by the first occurrence of the conodont *Palmatolepis triangularis*
83 (Fig. 2; Klapper et al., 1993; Over, 1997, 2002; see also Spalletta et al., 2017) and occurs
84 as a regionally continuous bed of black shale that is taken to be equivalent to the Upper
85 Kellwasser Horizon (Kelly et al., 2019; Cohen et al., 2021; Uveges et al., 2019).

86 **3 Methods**

87 Across the F–F boundary interval, black shales were sampled at a 2–5 cm
88 stratigraphic resolution. Above and below the F–F boundary, the black shale units were

89 sampled at a lower resolution of approximately 5–10 cm. Samples were powdered (~200
90 mesh) using a Zirconium dish and puck mill using a shatterbox.

91 *3.1 Total organic carbon and organic carbon isotope*

92 Total organic carbon (TOC) content and organic carbon isotope ($\delta^{13}\text{C}_{\text{org}}$)
93 determinations were analysed at the State Key Laboratory of Organic Geochemistry at
94 Guangzhou Institute of Geochemistry. Samples were acidified: ~1 g of powder was
95 mixed with 15 mL 2 N HCl and left for 24 h. Acid was decanted and then the samples
96 were rinsed three times with DI water to neutralize the acid. Samples were then dried in
97 an oven at 60 °C for 2–3 days until their weights are constant. The TOC measurements
98 were conducted using a Leco CS230 carbon/sulfur analyser. The samples were further
99 ground to fine powder using an agate pestle and mortar and loaded into tin capsules for
100 carbon isotope measurement. Carbon isotope values ($\delta^{13}\text{C}_{\text{org}}$) were analyzed using a
101 Thermo Delta XL Plus isotope ratio mass spectrometer. Data are reported in delta notation
102 (δ) in per mil (‰) relative to the Vienna Peedee Belemnite (VPDB). The analytical
103 uncertainty on internal standards throughout the analytical run was ± 0.09 ‰ (2σ , $n = 10$).

104 *3.2 Molecular organic geochemistry*

105 Polycyclic aromatic hydrocarbons (PAHs) and saturated hydrocarbons analyses
106 were conducted in the State Key Laboratory of Organic Geochemistry at Guangzhou
107 Institute of Geochemistry. Before analyses, all the glassware, aluminum foil, silica gel,
108 quartz sand and quartz wool were baked in an oven at 500 °C for 6 hours to remove

109 potential organic contaminants. Sample powders (~10 g) were extracted with mixture
110 solvents of dichloromethane/methanol (9:1, v/v) in a Soxhlet extractor for 72 hrs. The
111 extracts were then separated into saturated, aromatic, and polar fraction using silica gel
112 column chromatography (~15 cm height). The volume of the silica gel column was
113 determined by counting the liquid volume of *n*-hexane from the first aliquot loaded to the
114 first volume eluted (dead volume, 1dv). Then the saturated fraction was eluted using three
115 times column volume of *n*-hexane (3dv). The aromatic fraction was eluted with a 3dv
116 dichloromethane/*n*-hexane (1:1, v/v) solution. The polar fraction was eluted with
117 methanol (Song et al., 2020). The eluent fractions were then concentrated to a final
118 volume of 0.3 mL.

119 The PAHs were analyzed using a Shimadzu gas chromatography-mass spectrometry
120 (GC/MS-QP2010) with an electron impact ion source at 70 eV. The chromatograph was
121 equipped with a HP-5MS column (30 m × 0.25 mm, film thickness 0.25 μm).
122 Approximately 1 μL of each aromatic fraction was injected in splitless mode and operated
123 under electron ion source (-70 eV) in full scan mode (50–550 amu). High purity helium
124 was used as the carrier gas at a flow rate of 1 mL/min. The temperature of transfer line,
125 injector interface and ion source were set at 290 °C, 290 °C and 250 °C, respectively. The
126 initial oven temperature was set at 70 °C for 3 min, then raised to 290 °C at a rate of 3 °C/
127 min, followed by a 30 min hold. The identification of compounds was based on the
128 retention time with reference compounds and comparison of published data.

129 Quantification of the PAHs were achieved by comparing the measured peak areas to those
130 with known amounts of internal reference compounds (deuterated PAHs, including
131 naphthalene-d8, acenaphthene-d10, phenanthrene-d10, chrysene-d12 and perylene-d12)
132 that were added to the samples before extraction. The blank control recorded only the
133 reference material which recorded no significant contamination.

134 The same GC-MS instrument was used for the saturated fraction. Approximately 1
135 μL of each extract was injected in splitless mode and operated under electron ion source
136 (-70 eV) in full scan mode (50–550 amu). High purity helium was used as the carrier gas
137 at a flow rate of 1 mL/min. The temperature of transfer line, injector interface and ion
138 source were set at 290 °C, 290 °C and 250 °C, respectively. The initial oven temperature
139 was set at 70 °C for 3 min, then raised to 300 °C at a rate of 4 °C/ min, followed by a 20
140 min hold. The *n*-alkanes, pristane and phytane were quantified against the internal
141 standard *n*-C₃₆.

142 **4 Results**

143 *4.1 Organic carbon isotope stratigraphy*

144 A large positive carbon isotope excursion was detected in all three sections around
145 the F–F boundary. At the BMC section, the $\delta^{13}\text{C}_{\text{org}}$ values increase from $\sim -29.5\text{‰}$ at the bottom
146 of the section to a maximum value of -26.4‰ at the F–F boundary, and then decline to $\sim -27.1\text{‰}$
147 stratigraphically upwards. At the Irish Gulf section, $\delta^{13}\text{C}_{\text{org}}$ values gradually increase from -29.9‰
148 across the F–F boundary and reach a nadir of -27.3‰ about 70 cm above the F–F boundary, and

149 then the $\delta^{13}\text{C}_{\text{org}}$ values gradually drop to ~ -28.5 ‰ upwards. At the WCB section, $\delta^{13}\text{C}_{\text{org}}$ values
150 average ~ -29.7 ‰ below the F–F boundary and rise dramatically to -27 ‰ across the F–F boundary,
151 and then slowly drop to ~ -28.8 ‰ in the upper part of the section (Fig. 2).

152 *4.2 Polycyclic aromatic hydrocarbons*

153 In this study, phenanthrene (Phe), pyrene (Pyr), chrysene (Chy), benzofluoranthenes
154 (BF), benzo[e]pyrene (BeP), benzo[ghi]perylene (BPer) and coronene (Cor) were
155 chosen as wildfire proxies to track the biomass burning activity during the F–F interval
156 (Fig. 2, Table S1). Phenanthrene and chrysene are the dominant PAHs at all three sections
157 (generally over 75 % of the total PAHs abundance). Both the five and six ring PAHs
158 (benzofluoranthenes, benzo[e]pyrene, benzo[ghi]perylene, and coronene) have similar
159 trends with the three and four ring PAHs (phenanthrene, pyrene, chrysene).

160 PAHs concentrations were normalized to the TOC for the assessment of
161 contributions to sedimentary organic matter from forest fires (e.g., Killops and Massoud,
162 1992; Jiang et al., 1998; Marynowski and Simoneit, 2009; Boudinot and Sepúlveda,
163 2020). The detailed trends for the total PAHs concentrations were described below, and
164 the trends with individual PAHs are plotted in Figure 2 (Table S1). At the Beaver Meadow
165 Creek section, the total PAHs amounts increase from ~ 115 $\mu\text{g/g}$ TOC to 143 $\mu\text{g/g}$ TOC
166 and then drop slightly to ~ 105 $\mu\text{g/g}$ TOC, which then further increase to 135 $\mu\text{g/g}$ TOC
167 at ~ 15 cm below the F–F boundary. The total PAHs values then gradually drop across the
168 F–F boundary to 51.2 $\mu\text{g/g}$ TOC, and slowly increase to ~ 125 $\mu\text{g/g}$ TOC in the upper part

169 of the section. At the Irish Gulf section, the total PAHs concentrations increase from ~102
170 $\mu\text{g/g}$ TOC to 134 $\mu\text{g/g}$ TOC, and then decline to 95 $\mu\text{g/g}$ TOC, which then gradually
171 increase to ~128 $\mu\text{g/g}$ across the F–F boundary. The values then gradually drop to ~87
172 $\mu\text{g/g}$ TOC, which then increase to higher values of ~121 $\mu\text{g/g}$ TOC and remained at high
173 levels upward. At the Walnut Creek Bank section, the total PAHs values increase from a
174 low concentration of 42.6 $\mu\text{g/g}$ TOC to 106.8 $\mu\text{g/g}$ TOC immediately above the F–F
175 boundary, which then drop to 83.6 $\mu\text{g/g}$ TOC and further increase to 105.4 $\mu\text{g/g}$ TOC.
176 The total PAHs values then drop to slightly lower values upsection.

177 At the Beaver Meadow Creek section, the 6/3-ring ratios increase from 0.038 to
178 0.074 at the base of the section, which then decrease to 0.047 and remain relatively
179 constant at ~0.045 upward through the F–F boundary interval. At the Irish Gulf section,
180 the 6/3-ring ratios express a peak from 0.057 to 0.083 about 10 cm below the F–F
181 boundary. The 6/3-ring values then increase to 0.102 above the F–F boundary, which then
182 decrease to ~0.05 in the upper part of the section. At the Walnut Creek Bank section, the
183 6/3-ring ratios decline from 0.08 to 0.024 below the F–F boundary, which then increase
184 to 0.053 immediately above the F–F boundary. The 6/3-ring ratios values then decrease
185 to ~0.04 upsection (Fig. 2).

186 **5. Discussion**

187 *5.1 Evaluation of thermal maturity and weathering effect on PAHs*

188 In nature, PAHs are generated by incomplete combustion of organic materials (Lima et al.,
189 2005). It has been used as a well-established wildfire proxy and applied in several climatic and biotic
190 perturbation intervals in the Earth history (Finkelstein et al., 2005; Kaiho et al., 2021; Kaiho et al.,
191 2013; Marynowski and Filipiak, 2007). However, prior to interpreting of PAH data as a primary
192 proxy for wildfire events, potential alteration from secondary processes such as weathering and/or
193 thermal maturity need to be carefully evaluated (Marynowski et al., 2011). Previous thermal
194 maturity proxies of solid bitumen reflectance (BR_o , ~0.7 %) and T_{max} values (~445 °C) suggest a
195 low thermal maturity of the samples throughout these F–F sections (Liu et al., 2020). Furthermore,
196 there is no correlation between PAHs concentrations and thermal maturity proxies from saturates
197 (e.g., $T_s/[T_s + T_m]$ and $22S/[22S + 22R]C_{31}$ homohopane; Fig. 3), and highly pericondensed
198 compounds like benzofluoranthenes, benzo[e]pyrene, benzo[ghi]perylene and coronene are
199 minimally susceptible to thermal alteration and biodegradation (Jiang et al., 1998; Schmidt and
200 Noack, 2000). Further, early studies have demonstrated that pyrene, benzo[ghi]perylene, and
201 coronene are dominant types of PAHs derived from forest fires (Venkatessen and Dahl, 1989;
202 Killips and Massoud, 1992; Masclet et al., 1995; Arinobu et al., 1999), and their condensed
203 structures make them resistant to degradation (Killips and Massoud, 1992). Weathering processes
204 have been demonstrated to be able to alter the PAHs record (Marynowski et al., 2011). However,
205 in this study, fresh outcrop samples were collected and extra care has been taken to remove the
206 potential weathered surface. Furthermore, other geochemistry analyses such as osmium isotope
207 ($^{187}Os/^{188}Os$, or Os_i), which is extremely sensitive to weathering, have yielded geologically

208 meaningful Os_i values that are identical to Os_i values from core records (see Fig. 7 in Liu et al., 2020)
209 and are equivalent to Os_i values from other sections (Gordon et al., 2009; Harris et al., 2013; Jaffe
210 et al., 2002; Turgeon et al., 2007). Therefore, we consider the trends of PAHs compounds in the F–
211 F strata to reflect a primary depositional signature and might suggest enhanced frequency of wildfire
212 activity towards the F–F (Fig. 2). The appearance of inertinite from these sections further
213 demonstrate that the PAHs are of fire origin, although the inertinite and PAHs profiles do not
214 correlate (Fig. 2; Liu et al., 2020). The maximum concentrations of PAHs occur before the maximal
215 inertinite content (Fig. 2). This may be in a direct response to sea-level fall at the F–F boundary.
216 Thus, possibly more inertinite was transported to the sea due to the shorter transport distance. In
217 contrast, PAHs were transported via aerosols.

218 5.2 Wildfires across the F–F Interval

219 Although all PAHs are shown to have a combustion source (Lima et al., 2005), the distribution
220 of PAHs in the surrounding sediments are linked to the specific burning conditions, *e.g.*, the burning
221 of plant community material combined with the combustion temperature (Lima et al., 2005).
222 Moreover, the distribution of PAHs in the sedimentary record could be affected by the distance of
223 transportation and the form (particulate/gas) of the transportation (Masclat et al., 1988; 1995). For
224 example, benzo[e]pyrene and coronene are enriched in the particulate phase, whereas pyrene and
225 fluorene are dominant in the gas phase (Masclat et al., 1988; 1995). The precipitation of PAHs
226 during the transportation might also affect the final PAHs deposition/composition in the
227 sedimentary record (Masclat et al., 1988; 1995). Previous investigations have suggested that the

228 forest fire type during the F–F interval was a surface fire with burning temperature estimated
229 between 400 and 500 °C, rather than an intensive crown fire, based on inertinite reflectance value
230 of 1.74–3.16 %. The burning material is inferred to be herbaceous and shrubby material (Liu et al.,
231 2020). The heterogenous trends for each individual type of PAHs, and the different PAHs trends
232 for each of the investigated sections may be linked to the special heterogeneity of wildfires and their
233 burning temperatures, as well as the sections' distance from the land that the PAHs in the gas phase
234 may migrate further than those in the particulate phase (Fig. 2).

235 At the Walnut Creek Bank section, the PAHs generally show an increase in concentration
236 towards the F–F boundary, and the coronene concentration firstly decreases below the F–F and then
237 increases across the F–F boundary (Fig. 2). At the Irish Gulf section, most of the PAHs show an
238 increasing trend towards the F–F boundary, with phenanthrene, chrysene and coronene
239 expressing a small peak below the F–F boundary (Fig. 2). The increase in the concentrations of
240 pyrene, benzo[ghi]perylene, and coronene towards the F–F boundary at the Irish Gulf and Walnut
241 Creek Bank sections might suggest increased wildfire burning frequency during the F–F interval,
242 although the Beaver Meadow Creek section show a relatively constant profile of the PAHs
243 concentrations (Fig. 2). High burning temperature may generate more 6-ring PAHs compared with
244 three-ring PAHs, which could also be generated from weathering and burning of sedimentary
245 hydrocarbons (*e.g.*, coal; Belcher et al., 2009; Killops and Masoud, 1992, Finkelstein et al., 2005;
246 Belcher et al., 2009). Thus, the 6/3-ring ratio has been proven to be a useful proxy to reconstruct
247 high temperature biomass burning that occurs during forest fires, and reduce the influence of

248 changes related weathering and burning of sedimentary hydrocarbons (Boudinot and Sepúlveda,
249 2020). The 6/3-ring ratio increase towards the F–F boundary at the WCB and IG sections.
250 Moreover, an increase in the 6/3-ring ratio at the BMC section were also found, although it is slightly
251 stratigraphically lower than that of the IG and WCB sections. The latter support an increase in
252 frequency of wildfires and an increase in high temperature burning during the F–F interval. An
253 increase in PAHs abundance (Cor, BPer and BeP) has also been reported for two Belgium
254 sections and are interpreted to reflect enhanced wildfire events (Kaiho et al., 2013). The increase
255 of resistant PAHs degradation (pyrene, benzo[ghi]perylene, and coronene) and the 6/3-ring ratio
256 over the F–F interval further support the occurrence of wildfires and increased frequency towards
257 the F-F Boundary. Nonetheless, the exact scale (global, regional, or local) of wildfires during the
258 F–F interval remains unclear without further investigation of multiple F–F sections.

259 The ignition of wildfires could be caused by heat from natural lightning, volcanic activity,
260 meteorite impact and even sparks generated by rock fall, with lightning strikes considered to be the
261 most common ignition method (Glasspool and Scott, 2010). In the case of the wildfires
262 around the F–F interval, volcanism could have been an alternative source of ignition.
263 Increased mercury concentrations (which has been used as evidence for volcanic
264 activities by several researchers) have been reported from several F–F sections (Racki et
265 al., 2018; Kaiho et al., 2021; Liu et al., 2021; Zhao et al., 2022). Moreover, a bentonite layer
266 has also been reported below the F–F interval, which might indicate volcanism before the
267 F–F Boundary (Kaufmann *et al.*, 2004). It is worth to note that the dating of the F-F

268 boundary does not directly correlate with any major large igneous provinces ages, and Hg
269 enrichments might be driven by increased amounts of sulfides, organic matter and clay
270 minerals rather than volcanism (e.g., Percival et al., 2018, Shen et al., 2020). An increase
271 in coronene abundance for three carbonate-dominated F–F sections (Yangdi, China;
272 Sinsin, Belgium; Coumiac, France; with TOC generally less than 0.3 %) is interpreted to
273 be the product of high-temperature country rock heating caused by the sill emplacement
274 and/or large wildfires ignited by lava flows, rather than normal wildfires (Kaiho et al.,
275 2021). However, in the sections from this study, no Hg (Hg/TOC) spike is detected (Liu
276 et al., 2021), and thus the PAHs are likely produced by combustion from natural wildfires.

277 *5.3 Implications for elevated atmospheric oxygen level*

278 For terrestrial plant material to burn, a minimum pO_2 concentration of 16 % is
279 needed (Belcher et al., 2010). Below this level, regardless of the dryness of the organic
280 matter, wildfire activity cannot be sustained. In general, the higher the oxygen level, the
281 less effect the moisture content has on the ability for organic material to combust (Watson
282 and Lovelock, 2013). In the Late Devonian, readily available combustible terrestrial
283 organic matter comprised a developed plant community and even the appearance of small
284 forests (Stein et al., 2012). However, the F–F interval has been considered to be an
285 interval with few wildfire events due to suppression by low pO_2 level (~17 %, Scott and
286 Glasspool, 2006). The recovery of inertinite coupled with PAHs data in this study, further
287 suggests the occurrence of wildfires during the F–F interval (Fig. 2). The increased PAHs

288 concentration towards the FFB is consistent with an increase in pO_2 level over this
289 interval as suggested by different models (Krause et al., 2018; Lenton et al., 2018;
290 Schachat et al., 2018).

291 In addition to an increased pO_2 level, changes in aridity can make areas or intervals
292 more prone to wildfire events (Heimhofer et al., 2018). Plants tend to biosynthesize
293 longer plant cuticle wax chains to retain moisture within the leaf as a response to drier
294 climate (Eglinton and Hamilton, 1967). The average chain length (ACL) of plant wax n -
295 alkanes, as calculated by Eq. (1), has been shown to be an effective proxy for aridity (Carr
296 et al., 2014).

$$297 \text{ ACL} = \frac{([nC_{27}] * 27) + ([nC_{29}] * 29) + ([nC_{31}] * 31) + ([nC_{33}] * 33) + ([nC_{35}] * 35)}{[nC_{27}] + [nC_{29}] + [nC_{31}] + [nC_{33}] + [nC_{35}]} \quad (1)$$

299 However, it is noteworthy that cases have also been reported where ACL decreases
300 in response to increased aridity (Hoffmann et al., 2013). In addition, plant community
301 changes can also affect the changes in ACL (Bush and McInerney, 2013; Diefendorf et
302 al., 2011; Vogts et al., 2012). These factors all together make the interpretation of ACL
303 data complicated.

304 Regardless of cause, the average chain length (ACL) in all three sections remained
305 around 29, with the Beaver Meadow Creek (BMC) and Irish Gulf (IG) sections increasing
306 slightly to ~29.5 below the FFB (Fig. 4). This short stratigraphic interval would be too
307 brief for any plant community change. Rather, a transient change in aridity might be a

308 more reasonable interpretation for these minor increases in ACL. However, aridity change
309 cannot account for the trend in increasing PAHs abundance in this study (Fig. 4). Thus,
310 the increased PAHs abundance towards the FFB and above reflects enhanced wildfire
311 frequency caused by elevated pO_2 level, potentially aided by a transient increase in aridity.

312 In addition to being regulated by pO_2 levels, wildfires have been proposed to have a
313 positive feedback on the pO_2 level. As pO_2 level increases, wildfire intensity would
314 increase and thus more charcoal would be produced and buried. This enhanced carbon
315 burial would then further contribute to the rise of pO_2 levels (Rimmer et al., 2015).
316 Previously, the pO_2 level has been estimated to be 24–27 % (Liu et al., 2020). In addition
317 to a sharp rise in pO_2 , the ocean also experienced an episode of oxygenation across the
318 Devonian, as evidenced by near-present day level $\delta^{98}Mo$ values for euxinic samples (2.0 ‰
319 compared with the modern seawater value of 2.3 ‰; Dahl et al., 2010 and reference
320 therein). This indicates a synchronised rise in the atmospheric and oceanic oxygen contents
321 over the Devonian (Fig. 5) although experiencing a episode of anoxia across the F–F
322 interval (see below discussion).

323 *5.4 Implications for the Frasnian–Famenian mass extinction*

324 Wildfires have been proposed to destroy plant root systems and lead to enhanced
325 continental weathering, generate soot and aerosol, and affect the carbon cycle and climate,
326 which then are ultimately linked with major ocean anoxia or mass extinction events (*e.g.*,
327 Archibald et al., 2018). Increased runoff and transport of terrestrial organic matter,

328 including terrestrial-derived nutrients (*e.g.*, P and N) flux to the ocean have been observed
329 in response to modern and ancient wildfire events (Barkley et al., 2019). A slightly
330 enhanced terrestrial input was inferred from the relative abundance of plant wax
331 (calculated by $n\text{-C}_{27,29,31,33,35}/n\text{-C}_{17,19,21,27,29,31,33,35}$; Boudinot and Sepúlveda, 2020)
332 showing a minor increase below the FFB that correlates to the ACL increase in the more
333 proximal sections of BMC and IG. The pristane/phytane (Pr/Ph) ratio has been used as a
334 redox indicator (lower Pr/Ph ratios indicating reducing conditions and higher ratios
335 indicating more oxic conditions), as reducing conditions favor the conversion of the
336 phytanyl side chain of chlorophyll to phytane whereas oxic environments encourage the
337 conversion of phytanyl to pristane (Peters et al., 2005). However, the utility of this
338 biomarker is limited by multiple factors (Koopmas et al., 1999; Peters et al., 2005). For
339 example, the Pr/Ph ratio may also be affected by the source of organic matter, with an
340 increased flux of terrestrial organic matter resulting in an increase in the Pr/Ph value
341 (Song et al., 2020). In the investigated sections, the samples are dominated by marine
342 organic matter, with very limited terrestrial organic matter contribution (less than 2.2 %,
343 Liu et al., 2020). Thus, we carefully infer our Pr/Ph values here to reflect redox conditions.
344 In the studied sections, the Pr/Ph data generally remain constant around 1 throughout the
345 F–F interval. Further, isorenieratane and aryl isoprenoids produced by green sulfur
346 bacteria are considered to be robust proxies for photic zone euxinia (Summons and Powell,
347 1986). The presence of very low absolute amounts of aryl isoprenoids and isorenieratane

348 (near the detection limit) for the investigated sections (C_{13} – C_{22} aryl isoprenoids average
349 9.04, 3.37 and 10.98 $\mu\text{g/g}$ TOC for the BMC, IG, and WCB sections, respectively;
350 Haddad et al., 2016) are several orders of magnitude lower than those reported from
351 euxinic basins (*e.g.*, 2723 $\mu\text{g/g}$ TOC for C_{14} – C_{27} aryl isoprenoid during the
352 Changhsingian leading into the Permian–Triassic mass extinction event at the Meishan
353 section, South China; Cao et al., 2009). This further supports that the local marine redox
354 conditions in the Appalachian basin during the F–F interval were not persistently euxinic
355 (Boyer et al., 2014; Haddad et al., 2016, 2018; Kelly et al., 2019).

356 Ocean anoxia/euxinia has been frequently linked with the F–F mass extinction event.
357 Albeit not recorded in our study, widespread and intermittent ocean anoxia has been
358 reported for F–F sections globally. In contrast, the absence of evidence for ocean anoxia,
359 or even more oxygenated ocean, has been shown in several sections, such as Australia
360 (Becker et al., 1991; George et al., 2014), North America (Bratton et al., 1999; White et
361 al., 2018), and South China (Song et al., 2017) (see a review by Carmichael et al., 2019
362 for a summary of the redox states of global F–F sections). Heterogeneity in nutrient supply,
363 local depositional conditions, and the living organism species is expected within a global
364 ocean system for any interval of Earth history. Further high-resolution studies with
365 sections that have clear biostratigraphy characterization are needed for section correlation
366 and to determine the timing and locality of ocean anoxia, and to correlate ocean anoxia
367 with the F–F mass extinction event.

368 In addition, elevated nutrient supply from enhanced terrestrial input might have
369 boosted the marine productivity. Increased burial of marine organic matter and inert
370 carbon (*e.g.*, charcoal, soot) would have lead to a positive CIE and the drawdown of the
371 $p\text{CO}_2$, and cause climate cooling that may have ultimately contributed to the F–F event
372 (Averbuch et al., 2005; Huang et al., 2018; Joachimski and Buggisch, 2002; Song et al.,
373 2017). Paleontology studies suggest that faunas living in warm temperatures were
374 sensitive to cooling, and experienced more severe losses than faunas living in cooler water
375 temperatures (McGhee, 1996; Ma et al., 2016). For example, over 90% of all brachiopod
376 families from the low-latitude, tropical regions became extinct, in comparison with ~ 27%
377 brachiopods from the cooler waters (McGhee, 1996). Warm-adapted benthic ostracods
378 were also severely affected, whereas sponges and solitary rugose corals that lived in deep
379 water environments were less affected (Ma et al., 2016). After the F–F mass extinction,
380 faunas (*e.g.*, foraminifers) that previously populated high-latitude regions migrated to
381 low-latitude regions, with the low-latitude organisms that survived displaying a dramatic
382 decline in their biogeographic distribution (Kalvoda, 1990). In addition to the mass
383 extinction in the marine realm, research has shown that the F–F biotic crisis also affected
384 the terrestrial ecosystems to some extent (McGhee, 1996). The ecological selectivity of
385 the F–F biotic crisis is better explained by climate cooling. In summary, our organic
386 geochemistry data do not provide evidence for enhanced ocean anoxia in the Appalachian
387 basin, and whether ocean anoxia is a killing mechanism of the F–F mass extinction still

388 needs further research. The increased frequency of wildfires fit with the climate cooling
389 scenario across the F–F boundary interval.

390 **6 Conclusions**

391 The PAHs data from three F–F sections suggest enhanced wildfire activity around
392 the FFB (Fig. 2). The dominance of three-ring Phenanthrene indicates that the wildfire
393 has a low burning intensity. Average chain length data remained relatively constant at 29
394 for all three sections, and thus indicate relative aridity conditions were stable during this
395 time interval. The enhanced wildfire activity might be linked to an elevated atmospheric
396 oxygen level. Although a slightly increased terrestrial input was observed, no major
397 oceanic oxygen deficiency in the Appalachian basin is detected over the F–F interval by
398 Pr/Ph, albeit that widespread and intermittent ocean anoxia has been reported.
399 Nevertheless, our evidence for enhanced wildfire activity corroborates with the
400 hypothesis that $p\text{CO}_2$ drawdown and climate cooling that resulted from enhanced
401 mountain building and continental weathering might have led to the F–F biocrisis. This
402 interpretation seems more consistent with the pattern that shallow water species were
403 among those most severely affected.

404 **Acknowledgements**

405 We acknowledge the Natural Science Foundation of China (41925014) to HT,
406 (41790452) to JH, and the China Postdoctoral Science Foundation (20M682934) and
407 Director's Fund of Guangzhou Institute of Geochemistry, CAS to ZL.

408 **References**

- 409 Archibald, S., Lehmann, C.E.R., Belcher, C.M., Bond, W.J., Bradstock, R.A., Daniau,
410 A.L., Dexter, K.G., Forrestel, E.J., Greve, M., He, T., Higgins, S.I., Hoffmann,
411 W.A., Lamont, B.B., McGlenn, D.J., Moncrieff, G.R., Osborne, C.P., Pausas, J.G.,
412 Price, O., Ripley, B.S., Rogers, B.M., Schwilk, D.W., Simon, M.F., Turetsky, M.R.,
413 Van der Werf, G.R., Zanne, A.E. (2018) Biological and geophysical feedbacks with
414 fire in the Earth system. *Environmental Research Letters* 13, 033003.
- 415 Arinobu, T., Ishiwatari, R., Kaiho, K., Lamolda, M.A., 1999. Spike of pyrosynthetic
416 polycyclic aromatic hydrocarbons associated with an abrupt decrease in $\delta^{13}\text{C}$ of a
417 terrestrial biomarker at the Cretaceous-Tertiary boundary at Caravaca, Spain.
418 *Geology* 27, 723-726.
- 419 Averbuch, O., Tribovillard, N., Devleeschouwer, X., Riquier, L., Mistiaen, B., van
420 Vliet-Lanoe, B. (2005) Mountain building-enhanced continental weathering and
421 organic carbon burial as major causes for climatic cooling at the Frasnian-
422 Famennian boundary (c. 376 Ma)? *Terra Nova* 17, 25-34.
- 423 Barkley, A.E., Prospero, J.M., Mahowald, N., Hamilton, D.S., Pependorf, K.J., Oehlert,
424 A.M., Pourmand, A., Gatineau, A., Panechou-Pulcherie, K., Blackwelder, P.,
425 Gaston, C.J. (2019) African biomass burning is a substantial source of phosphorus
426 deposition to the Amazon, Tropical Atlantic Ocean, and Southern Ocean.
427 *Proceedings of the National Academy of Sciences* 116, 16216-16221.

428 Belcher, C.M., Finch, P., Collinson, M.E., Scott, A.C., Grassineau, N.V., 2009.
429 Geochemical evidence for combustion of hydrocarbons during the K-T impact
430 event. *Proceedings of the National Academy of Sciences* 106, 4112-4117.

431 Belcher, C.M., Yearsley, J.M., Hadden, R.M., McElwain, J.C., Rein, G. (2010) Baseline
432 intrinsic flammability of Earth's ecosystems estimated from paleoatmospheric
433 oxygen over the past 350 million years. *Proceedings of the National Academy of*
434 *Sciences* 107, 22448-22453.

435 Becker, R.T., House, M.R., Kirchgasser, W.T., Playford, P.E., 1991. Sedimentary and
436 faunal changes across the frasnian/famennian boundary in the canning basin of
437 Western Australia. *Historical Biology* 5, 183-196.

438 Bond, D., Wignall, P.B., Racki, G. (2004) Extent and duration of marine anoxia during
439 the Frasnian–Famennian (Late Devonian) mass extinction in Poland, Germany,
440 Austria and France. *Geological Magazine* 141, 173-193.

441 Bond, D.P.G., Wignall, P.B., 2008. The role of sea-level change and marine anoxia in
442 the Frasnian–Famennian (Late Devonian) mass extinction. *Palaeogeography,*
443 *Palaeoclimatology, Palaeoecology* 263, 107-118.

444 Boudinot, F.G., Sepúlveda, J. (2020) Marine organic carbon burial increased forest fire
445 frequency during Oceanic Anoxic Event 2. *Nature Geoscience* 13, 693-698.

446 Boyer, D.L., Haddad, E.E., Seeger, E.S., 2014. The Last Gasp: Trace Fossils Track
447 Deoxygenation Leading into the Frasnian-Famennian Extinction Event. *Palaios* 29,
448 646-651.

449 Boyer, D.L., Martinez, A.M., Evans, S.D., Cohen, P.A., Haddad, E.E., Pippenger, K.H.,
450 Love, G.D., Droser, M.L., 2021. Living on the edge: The impact of protracted

451 oxygen stress on life in the Late Devonian. *Palaeogeography, Palaeoclimatology,*
452 *Palaeoecology* 566, 110226.

453 Bratton, J.F., Berry, W.B.N., Morrow, J.R., 1999. Anoxia pre-dates Frasnian–
454 Famennian boundary mass extinction horizon in the Great Basin, USA.
455 *Palaeogeography, Palaeoclimatology, Palaeoecology* 154, 275-292.

456 Bush, R.T., McInerney, F.A. (2013) Leaf wax n-alkane distributions in and across
457 modern plants: Implications for paleoecology and chemotaxonomy. *Geochimica et*
458 *Cosmochimica Acta* 117, 161-179.

459 Cao, C., Love, G.D., Hays, L.E., Wang, W., Shen, S., Summons, R.E., 2009.
460 Biogeochemical evidence for euxinic oceans and ecological disturbance presaging
461 the end-Permian mass extinction event. *Earth and Planetary Science Letters* 281,
462 188-201.

463 Carmichael, S.K., Waters, J.A., Suttner, T.J., Kido, E., DeReuil, A.A., 2014. A new
464 model for the Kellwasser Anoxia Events (Late Devonian): Shallow water anoxia
465 in an open oceanic setting in the Central Asian Orogenic Belt. *Palaeogeography,*
466 *Palaeoclimatology, Palaeoecology* 399, 394-403.

467 Carmichael, S.K., Waters, J.A., Königshof, P., Suttner, T.J., Kido, E., 2019.
468 Paleogeography and paleoenvironments of the Late Devonian Kellwasser event: A
469 review of its sedimentological and geochemical expression. *Global and Planetary*
470 *Change* 183, 102984.

471 Carr, A.S., Boom, A., Grimes, H.L., Chase, B.M., Meadows, M.E., Harris, A. (2014)
472 Leaf wax n-alkane distributions in arid zone South African flora: Environmental
473 controls, chemotaxonomy and palaeoecological implications. *Organic*
474 *Geochemistry* 67, 72-84.

475 Claeys, P., Casier, J.-G., Margolis, S.V. (1992) Microtektites and Mass Extinctions:
476 Evidence for a Late Devonian Asteroid Impact. *Science* 257, 1102-1104.

477 Cohen, P.A., Junium, C.K., King Phillips, E., Uveges, B.T., 2021. Carbon cycle
478 dynamics and ecology revealed by the carbon isotopic composition of single
479 organic microfossils during the Late Devonian Biotic Crisis. *Geobiology* n/a.

480 Copper, P., 2002. Reef development at the Frasnian/Famennian mass extinction
481 boundary. *Palaeogeography, Palaeoclimatology, Palaeoecology* 181, 27-65.

482 Dahl, T.W., Hammarlund, E.U., Anbar, A.D., Bond, D.P.G., Gill, B.C., Gordon, G.W.,
483 Knoll, A.H., Nielsen, A.T., Schovsbo, N.H., Canfield, D.E. (2010) Devonian rise
484 in atmospheric oxygen correlated to the radiations of terrestrial plants and large
485 predatory fish. *Proceedings of the National Academy of Sciences* 107, 17911-
486 17915.

487 Diefendorf, A.F., Freeman, K.H., Wing, S.L., Graham, H.V. (2011) Production of n-
488 alkyl lipids in living plants and implications for the geologic past. *Geochimica et*
489 *Cosmochimica Acta* 75, 7472-7485.

490 Eglinton, G., Hamilton, R.J. (1967) Leaf Epicuticular Waxes. *Science* 156, 1322-1335.

491 Finkelstein, D.B., Pratt, L.M., Curtin, T.M., Brassel, S.C., 2005. Wildfires and seasonal
492 aridity recorded in Late Cretaceous strata from south-eastern Arizona, USA.
493 *Sedimentology* 52, 587-599.

494 George, A.D., Chow, N., Trinajstic, K.M., 2014. Oxidic facies and the Late Devonian
495 mass extinction, Canning Basin, Australia. *Geology* 42, 327-330.

496 Glasspool, I.J., Scott, A.C., Waltham, D., Pronina, N., Shao, L. (2015) The impact of
497 fire on the Late Paleozoic Earth system. *Frontiers in Plant Science* 6.

498 Glasspool, I.J., Scott, A.C. (2010) Phanerozoic concentrations of atmospheric oxygen
499 reconstructed from sedimentary charcoal. *Nature Geoscience* 3, 627.

500 Gordon, G.W., Rockman, M., Turekian, K.K., Over, J. (2009) Osmium isotopic
501 evidence against an impact at the Frasnian-Famennian boundary. 309, 420-430.

502 Haddad, E.E., Tuite, M.L., Martinez, A.M., Williford, K., Boyer, D.L., Droser, M.L.,
503 Love, G.D., 2016. Lipid biomarker stratigraphic records through the Late Devonian
504 Frasnian/Famennian boundary: Comparison of high- and low-latitude
505 epicontinental marine settings. *Organic Geochemistry* 98, 38-53.

506 Haddad, E.E., Boyer, D.L., Droser, M.L., Lee, B.K., Lyons, T.W., Love, G.D., 2018.
507 Ichnofabrics and chemostratigraphy argue against persistent anoxia during the
508 Upper Kellwasser Event in New York State. *Palaeogeography, Palaeoclimatology,
509 Palaeoecology* 490, 178-190.

510 Harris, N.B., Mnich, C.A., Selby, D., Korn, D. (2013) Minor and trace element and Re-
511 Os chemistry of the Upper Devonian Woodford Shale, Permian Basin, west Texas:
512 Insights into metal abundance and basin processes. *Chemical Geology* 356, 76-93.

513 Heimhofer, U., Wucherpfennig, N., Adatte, T., Schouten, S., Schneebeli-Hermann, E.,
514 Gardin, S., Keller, G., Kentsch, S., Kujau, A. (2018) Vegetation response to
515 exceptional global warmth during Oceanic Anoxic Event 2. *Nature
516 Communications* 9, 3832.

517 Hoffmann, B., Kahmen, A., Cernusak, L.A., Arndt, S.K., Sachse, D. (2013) Abundance
518 and distribution of leaf wax n-alkanes in leaves of Acacia and Eucalyptus trees
519 along a strong humidity gradient in northern Australia. *Organic Geochemistry* 62,
520 62-67.

521 Huang, C., Joachimski, M.M., Gong, Y. (2018) Did climate changes trigger the Late
522 Devonian Kellwasser Crisis? Evidence from a high-resolution conodont $\delta^{18}\text{O}_{\text{PO}_4}$
523 record from South China. *Earth and Planetary Science Letters* 495, 174-184.

524 Jaffe, L.A., Peucker-Ehrenbrink, B., Petsch, S.T. (2002) Mobility of rhenium, platinum
525 group elements and organic carbon during black shale weathering. *Earth and*
526 *Planetary Science Letters* 198, 339-353.

527 Jiang, C., Alexander, R., Kagi, R.I., Murray, A.P. (1998) Polycyclic aromatic
528 hydrocarbons in ancient sediments and their relationships to palaeoclimate.
529 *Organic Geochemistry* 29, 1721-1735.

530 Joachimski, M.M., Breisig, S., Buggisch, W., Talent, J.A., Mawson, R., Gereke, M.,
531 Morrow, J.R., Day, J., Weddige, K., 2009. Devonian climate and reef evolution:
532 Insights from oxygen isotopes in apatite. *Earth and Planetary Science Letters* 284,
533 599-609.

534 Johnson, J.G., Klapper, G., Sandberg, C.A. (1985) Devonian Eustatic Fluctuations in
535 Euramerica. *Geological Society of America Bulletin* 96, 567-587.

536 Joachimski, M.M., Buggisch, W., 2002. Conodont apatite $\delta^{18}\text{O}$ signatures indicate
537 climatic cooling as a trigger of the Late Devonian mass extinction. *Geology* 30,
538 711-714.

539 Kaiho, K., Miura, M., Tezuka, M., Hayashi, N., Jones, D.S., Oikawa, K., Casier, J.-G.,
540 Fujibayashi, M., Chen, Z.-Q. (2021) Coronene, mercury, and biomarker data
541 support a link between extinction magnitude and volcanic intensity in the Late
542 Devonian. *Global and Planetary Change* 199, 103452.

543 Kaiho, K., Yatsu, S., Oba, M., Gorjan, P., Casier, J.-G., Ikeda, M. (2013) A forest fire
544 and soil erosion event during the Late Devonian mass extinction. *Palaeogeography,*
545 *Palaeoclimatology, Palaeoecology* 392, 272-280.

546 Kalvoda, J., 1990. Late Devonian — Early Carboniferous paleobiogeography of benthic
547 Foraminifera and climatic oscillations, in: Kauffman, E.G., Walliser, O.H. (Eds.),
548 *Extinction Events in Earth History*. Springer Berlin Heidelberg, Berlin, Heidelberg,
549 pp. 183-187.

550 Kaufmann, B., Trapp, E., Mezger, K. (2004) The numerical age of the upper Frasnian
551 (Upper Devonian) Kellwasser horizons: A new U-Pb zircon date from Steinbruch
552 Schmidt (Kellerwald, Germany). *The Journal of Geology* 112, 495-501.

553 Kelly, A.A., Cohen, P.A., Boyer, D.L., 2019. Tiny Keys to Unlocking the Kellwasser
554 Events: Detailed Characterization of Organic Walled Microfossils Associated with
555 Extinction in Western New York State. *Palaios* 34, 96-104.

556 Klapper, G., Feist, R., Becker, R.T., House, M.R. (1993) Definition of the Frasnian
557 Famennian Stage Boundary. *Episodes* 16, 433-441.

558 Killops, S.D., Massoud, M.S., 1992. Polycyclic aromatic hydrocarbons of pyrolytic
559 origin in ancient sediments: evidence for Jurassic vegetation fires. *Organic*
560 *Geochemistry* 18, 1-7.

561 Koopmans, M.P., Rijkstra, W.I.C., Klapwijk, M.M., de Leeuw, J.W., Lewan, M.D.,
562 Sinninghe Damsté, J.S., 1999. A thermal and chemical degradation approach to
563 decipher pristane and phytane precursors in sedimentary organic matter. *Organic*
564 *Geochemistry* 30, 1089-1104.

565 Krause, A.J., Mills, B.J.W., Zhang, S., Planavsky, N.J., Lenton, T.M., Poulton, S.W.
566 (2018) Stepwise oxygenation of the Paleozoic atmosphere. *Nature*
567 *Communications* 9, 4081.

568 Lash, G.G. (2017) A multiproxy analysis of the Frasnian-Famennian transition in
569 western New York State, U.S.A. *Palaeogeography, Palaeoclimatology,*
570 *Palaeoecology* 473, 108-122.

571 Lenton, T.M., Daines, S.J., Mills, B.J.W. (2018) COPSE reloaded: An improved model
572 of biogeochemical cycling over Phanerozoic time. *Earth-Science Reviews* 178, 1-
573 28.

574 Lima, A.L.C., Farrington, J.W., Reddy, C.M. (2005) Combustion-Derived Polycyclic
575 Aromatic Hydrocarbons in the Environment—A Review. *Environmental Forensics*
576 6, 109-131.

577 Liu, Z., Percival, L.M.E., Vandeputte, D., Selby, D., Claeys, P., Over, D.J., Gao, Y.,
578 2021. Upper Devonian mercury record from North America and its implications
579 for the Frasnian–Famennian mass extinction. *Palaeogeography, Palaeoclimatology,*
580 *Palaeoecology* 576, 110502.

581 Liu, Z., Selby, D., Hackley, P.C., Over, D.J. (2020) Evidence of wildfires and elevated
582 atmospheric oxygen at the Frasnian–Famennian boundary in New York (USA):
583 Implications for the Late Devonian mass extinction. *GSA Bulletin*. 132(9-10):
584 2043-2054.

585 Lu, M., Lu, Y., Ikejiri, T., Sun, D., Carroll, R., Blair, E.H., Algeo, T.J., Sun, Y., 2021.
586 Periodic oceanic euxinia and terrestrial fluxes linked to astronomical forcing during
587 the Late Devonian Frasnian–Famennian mass extinction. *Earth and Planetary*
588 *Science Letters* 562, 116839.

589 Ma, X., Gong, Y., Chen, D., Racki, G., Chen, X., Liao, W., 2016. The Late Devonian
590 Frasnian–Famennian Event in South China — Patterns and causes of extinctions,
591 sea level changes, and isotope variations. *Palaeogeography, Palaeoclimatology,*
592 *Palaeoecology* 448, 224-244.

593 Marynowski, L., Filipiak, P., 2007. Water column euxinia and wildfire evidence during
594 deposition of the Upper Famennian Hangenberg event horizon from the Holy Cross
595 Mountains (central Poland). *Geological Magazine* 144, 569-595.

596 Marynowski, L., Simoneit, B.R.T., 2009. Widespread Upper Triassic to Lower Jurassic
597 Wildfire Records from Poland: Evidence from Charcoal and Pyrolytic Polycyclic
598 Aromatic Hydrocarbons. *Palaios* 24, 785-798.

599 Marynowski, L., Kurkiewicz, S., Rakociński, M., Simoneit, B.R.T. (2011) Effects of
600 weathering on organic matter: I. Changes in molecular composition of extractable
601 organic compounds caused by paleoweathering of a Lower Carboniferous
602 (Tournaisian) marine black shale. *Chemical Geology* 285, 144-156.

603 Masclet, P., Cachier, H., Lioussé, C., Wortham, H., 1995. Emissions of Polycyclic
604 aromatic hydrocarbons by savanna fires. *Journal of Atmospheric Chemistry* 22, 41-
605 54.

606 Masclet, P., Pistikopoulos, P., Beyne, S., Mouvier, G., 1988. Long range transport and
607 gas/particle distribution of polycyclic aromatic hydrocarbons at a remote site in the
608 Mediterranean Sea. *Atmospheric Environment (1967)* 22, 639-650.

609 McGhee, G.R., 1996. The late Devonian mass extinction: the Frasnian/Famennian crisis.
610 Columbia University Press.

611 Over, D.J. (1997) Conodont biostratigraphy of the Java Formation (Upper Devonian)
612 and the Frasnian-Famennian boundary in western New York State. In: Klapper, G.,

613 Murphy, M.A., and Talent, J.A. Eds.), Paleozoic Sequence Stratigraphy,
614 Biostratigraphy, and Biogeography: Studies in Honor of J. Granville ("Jess")
615 Johnson. Geological Society of America, 161-177.

616 Over, D.J. (2002) The Frasnian/Famennian boundary in central and eastern United
617 States. *Palaeogeography, Palaeoclimatology, Palaeoecology* 181, 153-169.

618 Percival, L.M.E., Davies, J.H.F.L., Schaltegger, U., De Vleeschouwer, D., Da Silva,
619 A.C., Föllmi, K.B., 2018. Precisely dating the Frasnian–Famennian boundary:
620 implications for the cause of the Late Devonian mass extinction. *Scientific Reports*
621 8, 9578.

622 Peters, K.E., Peters, K.E., Walters, C.C., Moldowan, J., 2005. *The biomarker guide*.
623 Cambridge University Press.

624 Racki, G., Rakociński, M., Marynowski, L., Wignall, P.B., 2018. Mercury enrichments
625 and the Frasnian-Famennian biotic crisis: A volcanic trigger proved? *Geology* 46,
626 543-546.

627 Rimmer, S.M., Hawkins, S.J., Scott, A.C., Cressler, W.L. (2015) The rise of fire: Fossil
628 charcoal in late Devonian marine shales as an indicator of expanding terrestrial
629 ecosystems, fire, and atmospheric change. *American Journal of Science* 315, 713-
630 733.

631 Sageman, B.B., Murphy, A.E., Werne, J.P., Ver Straeten, C.A., Hollander, D.J., Lyons,
632 T.W. (2003) A tale of shales: the relative roles of production, decomposition, and
633 dilution in the accumulation of organic-rich strata, Middle–Upper Devonian,
634 Appalachian basin. *Chemical Geology* 195, 229-273.

635 Schmidt, M.W.I., Noack, A.G. (2000) Black carbon in soils and sediments: Analysis,
636 distribution, implications, and current challenges. *Global Biogeochemical Cycles*
637 14, 777-793.

638 Schachat, S.R., Labandeira, C.C., Saltzman, M.R., Cramer, B.D., Payne, J.L., Boyce,
639 C.K. (2018) Phanerozoic pO₂ and the early evolution of terrestrial animals. *Proc.*
640 *R. Soc. B* 285, 20172631.

641 Scott, A.C., Glasspool, I.J. (2006) The diversification of Paleozoic fire systems and
642 fluctuations in atmospheric oxygen concentration. *Proceedings of the National*
643 *Academy of Sciences* 103, 10861-10865.

644 Shen, W., Sun, Y., Lin, Y., Liu, D., Chai, P. (2011) Evidence for wildfire in the Meishan
645 section and implications for Permian–Triassic events. *Geochimica et*
646 *Cosmochimica Acta* 75, 1992-2006.

647 Shen, J., Feng, Q., Algeo, T.J., Liu, J., Zhou, C., Wei, W., Liu, J., Them, T.R., Gill, B.C.,
648 Chen, J., 2020. Sedimentary host phases of mercury (Hg) and implications for use
649 of Hg as a volcanic proxy. *Earth and Planetary Science Letters* 543, 116333.

650 Song, H., Song, H., Algeo, T.J., Tong, J., Romaniello, S.J., Zhu, Y., Chu, D., Gong, Y.,
651 Anbar, A.D. (2017) Uranium and carbon isotopes document global-ocean redox-
652 productivity relationships linked to cooling during the Frasnian-Famennian mass
653 extinction. *Geology* 45, 887-890.

654 Song, Y., Gilleaudeau, G.J., Algeo, T.J., Over, D.J., Lyons, T.W., Anbar, A.D., Xie, S.
655 (2020) Biomarker evidence of algal-microbial community changes linked to redox
656 and salinity variation, Upper Devonian Chattanooga Shale (Tennessee, USA). *GSA*
657 *Bulletin*. <https://doi.org/10.1130/B35543.1>

658 Spalletta, C., Perri, M.C., Over, D.J., Corradini, C., 2017, Famennian (Upper Devonian)
659 conodont zonation: revised global standard: *Bulletin of Geosciences*, v. 92, p. 31–
660 57.

661 Stanley, S.M. (2016) Estimates of the magnitudes of major marine mass extinctions in
662 earth history. *Proc Natl Acad Sci USA* 113, E6325-E6334.

663 Stein, W.E., Berry, C.M., Hernick, L.V., Mannolini, F. (2012) Surprisingly complex
664 community discovered in the mid-Devonian fossil forest at Gilboa. *Nature* 483, 78.

665 Summons, R.E., Powell, T.G., 1986. Chlorobiaceae in Palaeozoic seas revealed by
666 biological markers, isotopes and geology. *Nature* 319, 763-765.

667 Turgeon, S.C., Creaser, R.A., Algeo, T.J. (2007) Re–Os depositional ages and seawater
668 Os estimates for the Frasnian–Famennian boundary: Implications for weathering
669 rates, land plant evolution, and extinction mechanisms. *Earth and Planetary Science*
670 *Letters* 261, 649-661.

671 Uveges, B.T., Junium, C.K., Boyer, D.L., Cohen, P.A., Day, J.E., 2019. Biogeochemical
672 controls on black shale deposition during the Frasnian-Famennian biotic crisis in
673 the Illinois and Appalachian Basins, USA, inferred from stable isotopes of nitrogen
674 and carbon. *Palaeogeography, Palaeoclimatology, Palaeoecology* 531, 108787.

675 Venkatesan, M.I., Dahl, J., 1989. Organic geochemical evidence for global fires at the
676 Cretaceous/Tertiary boundary. *Nature* 338, 57-60.

677 Vogts, A., Schefuß, E., Badewien, T., Rullkötter, J. (2012) n-Alkane parameters from a
678 deep sea sediment transect off southwest Africa reflect continental vegetation and
679 climate conditions. *Organic Geochemistry* 47, 109-119.

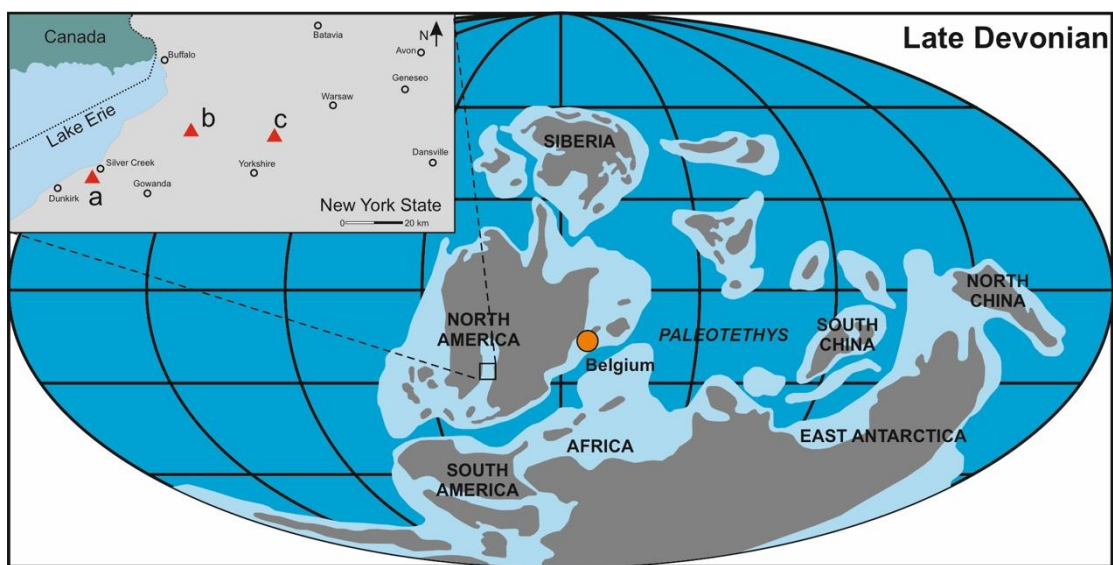
680 Watson, A.J., Lovelock, J.E. (2013) The Dependence of Flame Spread and Probability
681 of Ignition on Atmospheric Oxygen, *Fire Phenomena and the Earth System*, 273-
682 287.

683 White, D.A., Elrick, M., Romaniello, S., Zhang, F., 2018. Global seawater redox trends
684 during the Late Devonian mass extinction detected using U isotopes of marine
685 limestones. *Earth and Planetary Science Letters* 503, 68-77.

686 Zhao, H., Shen, J., Algeo, T.J., Racki, G., Chen, J., Huang, C., Song, J., Qie, W., Gong,
687 Y., 2022. Mercury isotope evidence for regional volcanism during the Frasnian-
688 Famennian transition. *Earth and Planetary Science Letters* 581, 117412.

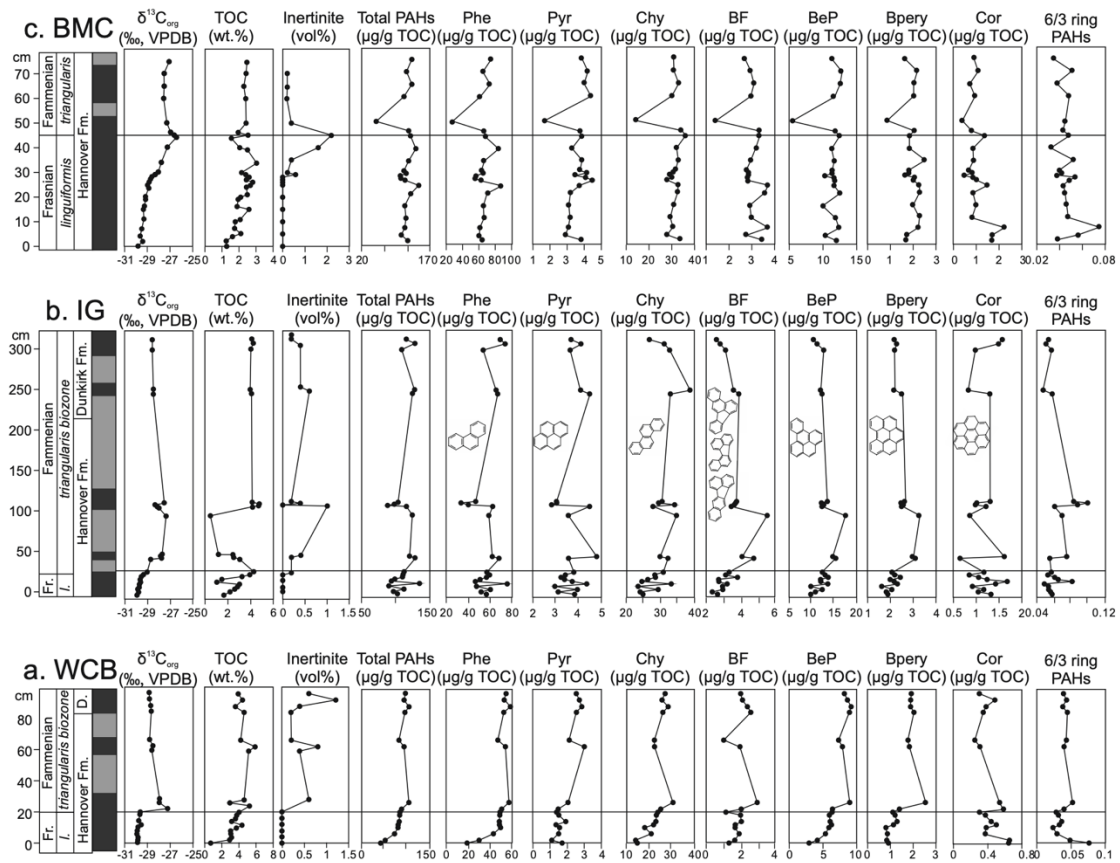
689 **Figures**

690 **Figure 1.** Paleogeography map showing location of the Appalachian Basin (open square)
691 in North America (after Liu et al., 2020). Inserted map shows the present-day New York
692 State sample locations – a: Walnut Creek Bank, b: Irish Gulf, c: Beaver Meadow Creek).
693 The orange circle represents the Belgium Frasnian–Famennian sections where a wildfire
694 event at the F–F boundary is also inferred (Kaiho et al., 2013).



695

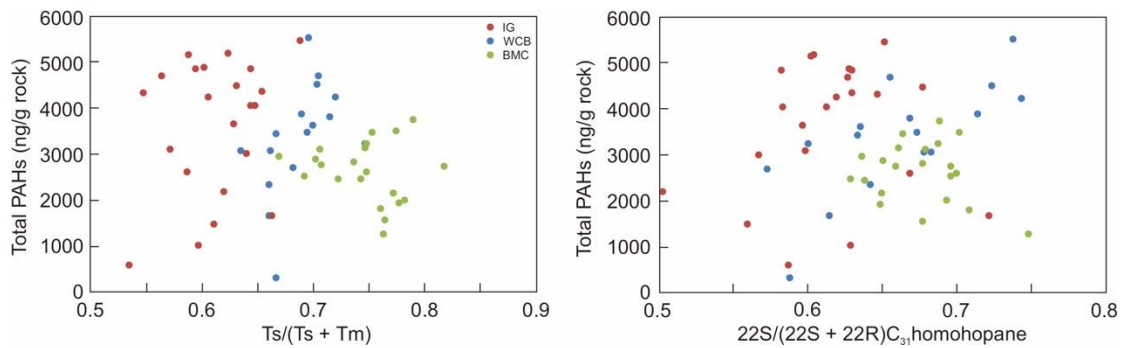
696 **Figure 2.** $\delta^{13}\text{C}_{\text{org}}$ stratigraphy and biomarkers from three F–F sections, New York State,
 697 USA. Abbreviations: Phe, phenanthrene; Pyr, pyrene; Chy, chrysene; BF,
 698 benzofluoranthenes; BeP, benzo[e]pyrene; BPerly, benzo[ghi]perylene; Cor, coronene;
 699 PWRA, plant wax relative abundance; ACL, average chain length. Inertinite abundance
 700 data are from Liu et al. (2020). a: Walnut Creek Bank (WCB); b: Irish Gulf (IG); c: Beaver
 701 Meadow Creek (BMC).



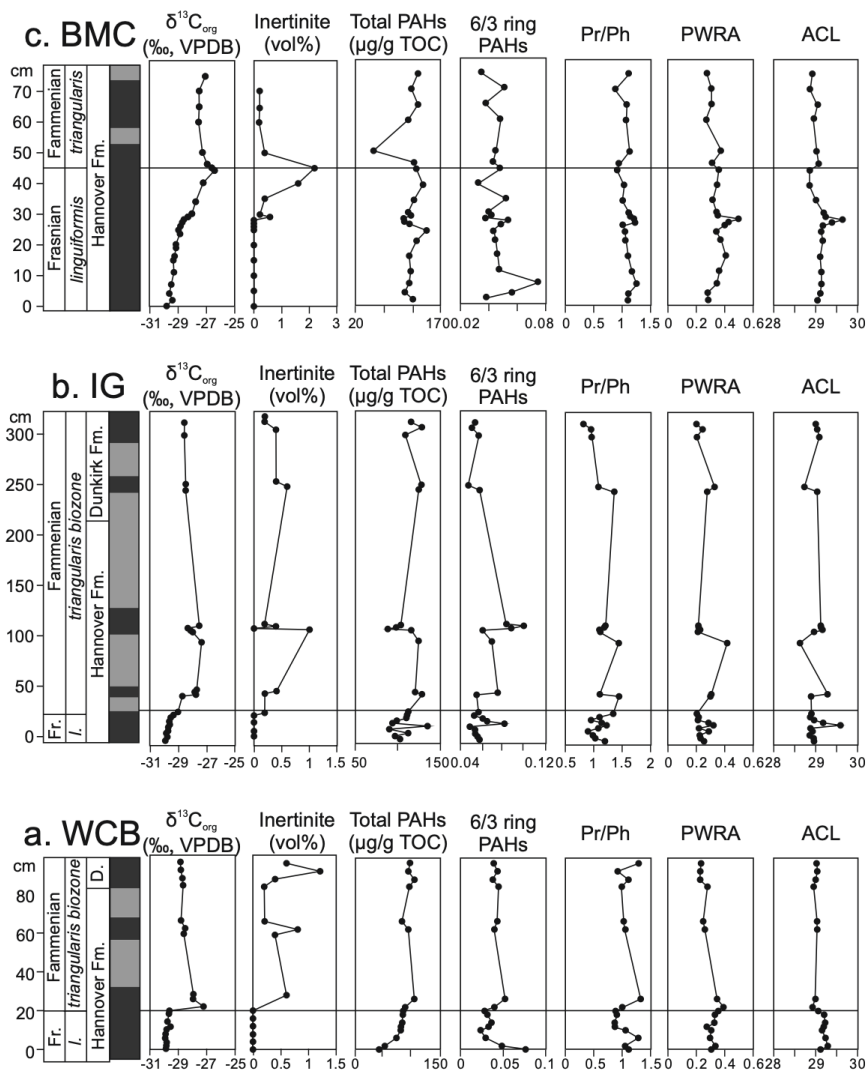
702

703 **Fig. 3** Cross plots for total PAHs concentrations and thermal maturity parameters. WCB:

704 Walnut Creek Bank (blue), IG: Irish Gulf (red), BMC: Beaver Meadow Creek (green).



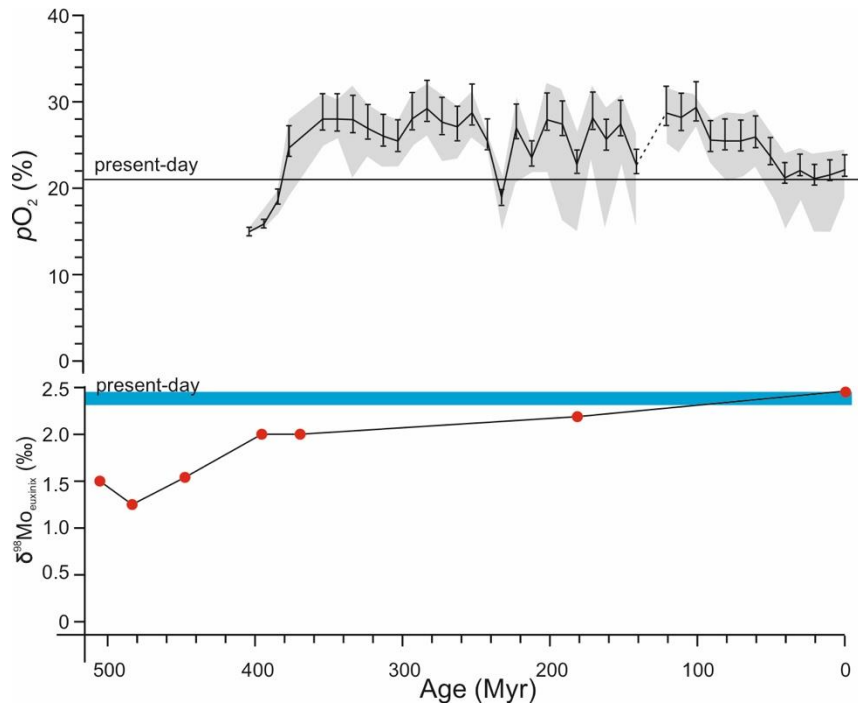
706 **Figure 4.** Biomarkers of plant wax relative abundance (PWRA), average chain length
 707 (ACL), and pristane/phytane ratio (Pr/Ph) from three F–F sections, New York State, USA.
 708 a: Walnut Creek Bank (WCB); b: Irish Gulf (IG); c: Beaver Meadow Creek (BMC).
 709 Inertinite abundance data are from Liu et al. (2020). See text for discussion.



710

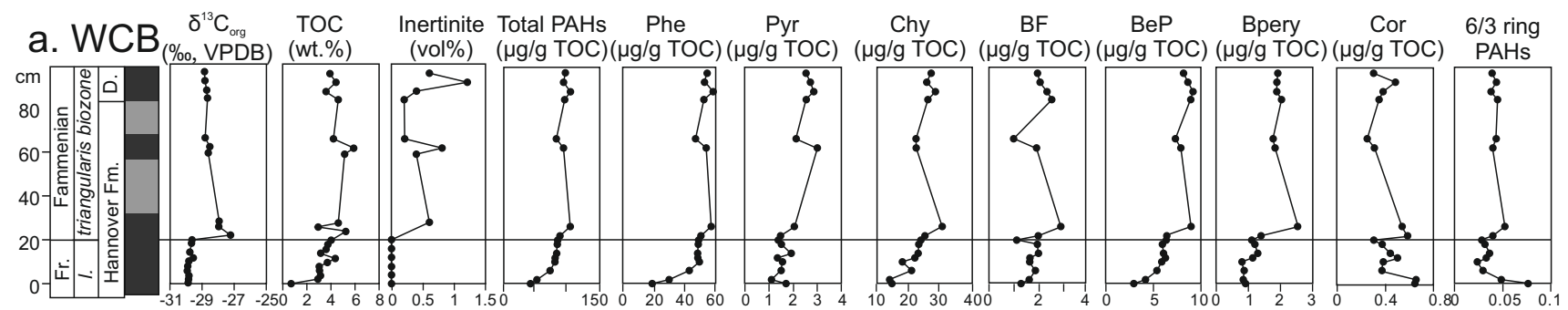
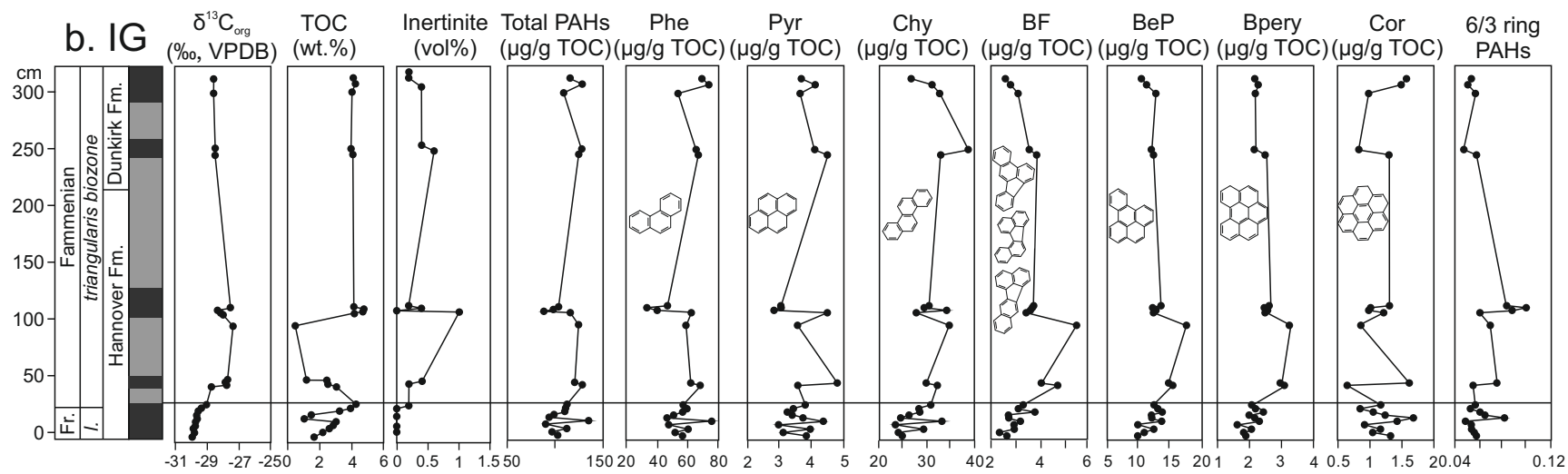
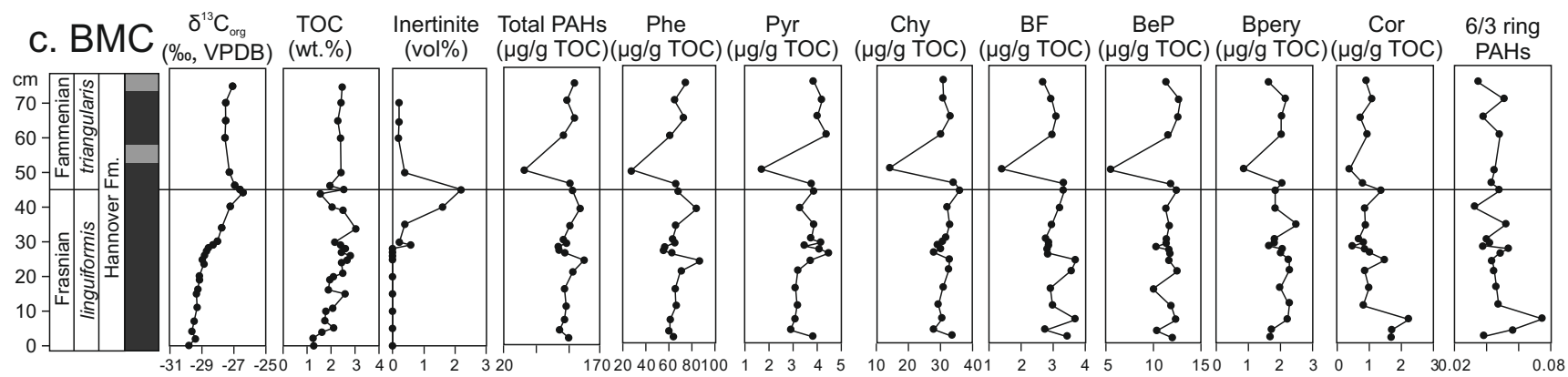
711 **Figure 5.** Evolution curve for atmospheric oxygen level (Liu et al., 2020) and Mo isotope

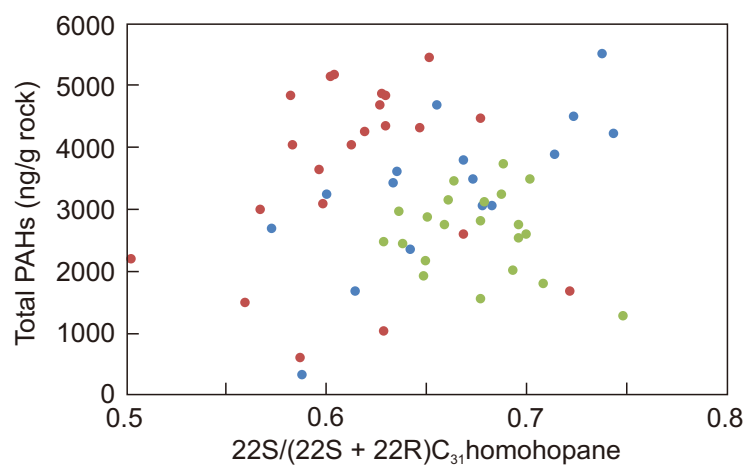
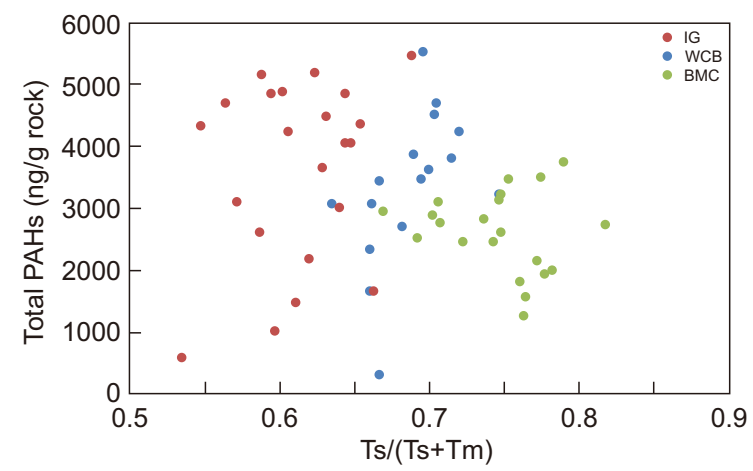
712 values of euxinic samples (Dahl et al., 2010). See text for discussion.

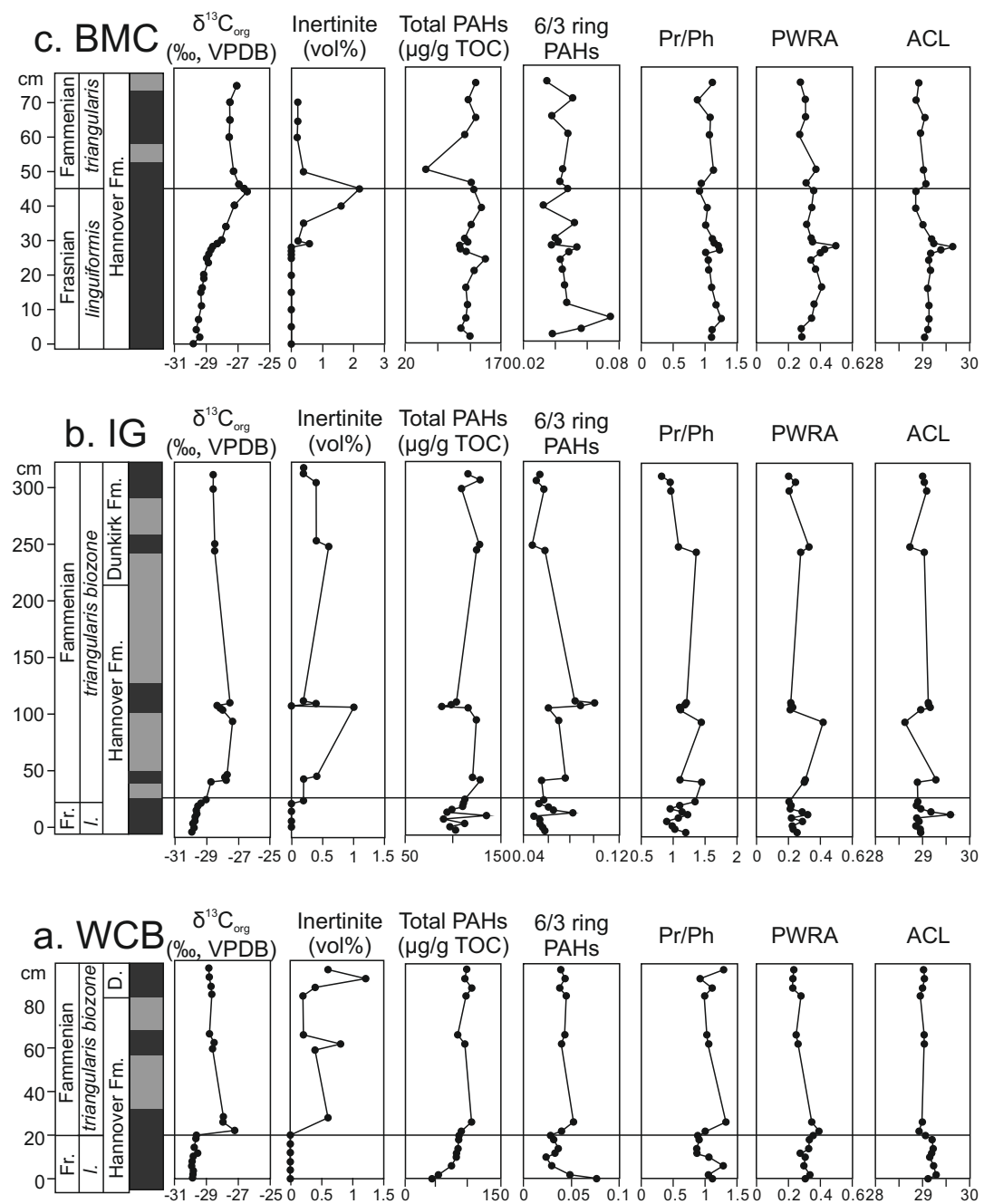


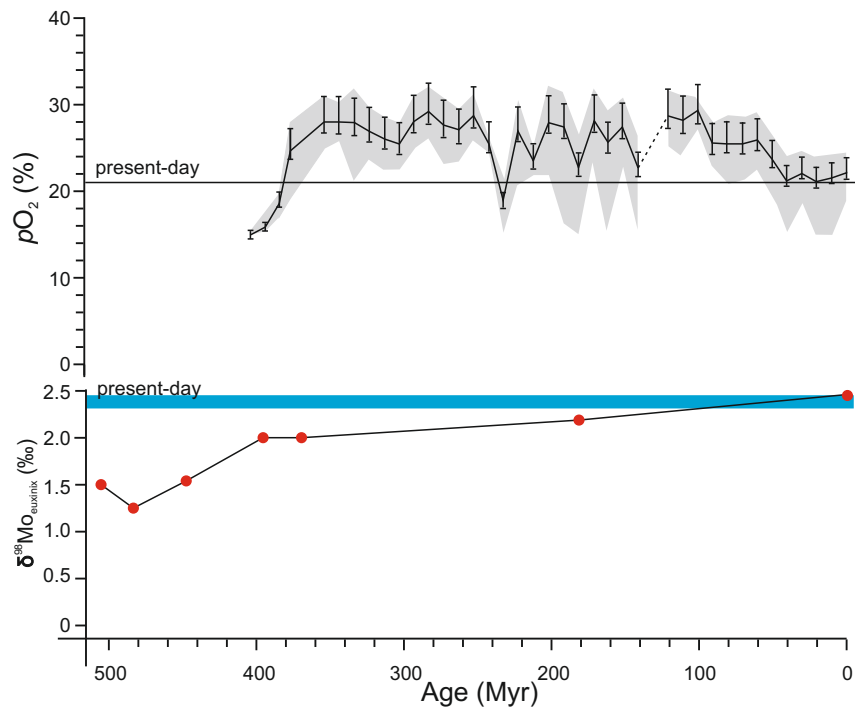
713











Conflict of Interest

The authors declare no conflict of interest. This manuscript has not been submitted and will not be submitted to any other journals while it is under review for *Global and Planetary Change*.